

Chiral and Color-superconducting Phase Transitions with Vector Interaction in a Simple Model

Masakiyo KITAZAWA^{a*)}, Tomoi KOIDE^{b**)}, Teiji KUNIHIRO^{b***)} and Yukio
NEMOTO^{c†)}

^a *Department of Physics, Kyoto university, Kyoto 606-8502, Japan*

^b *Yukawa Institute for Theoretical Physics, Kyoto University, Kyoto
606-8502, Japan*

^c *RIKEN BNL Research Center, BNL, Upton, NY 11973*

^{*)} masky@ruby.scphys.kyoto-u.ac.jp

^{**)} tkoide@yukawa.kyoto-u.ac.jp

^{***)} kunihiro@yukawa.kyoto-u.ac.jp

^{†)} nemoto@bnl.gov

Abstract

We investigate effects of the vector interaction on chiral and color superconducting (CSC) phase transitions at finite density and temperature in a simple Nambu-Jona-Lasinio model. It is shown that the repulsive density-density interaction coming from the vector term, which is present in the effective chiral models but has been omitted, enhances the competition between the chiral symmetry breaking (χ SB) and CSC phase transition, and thereby makes the thermodynamic potential have a shallow minimum over a wide range of values of the correlated chiral and CSC order parameters. We find that when the vector coupling is increased, the first order transition between the χ SB and CSC phases becomes weaker, and the coexisting phase in which both the chiral and color-gauge symmetry are dynamically broken comes to exist over a wider range of the density and temperature. We also show that there can exist two endpoints, which are tricritical points in the chiral limit, along the critical line of the first order transition in some range of values of the vector coupling. Although our analysis is based on a simple model, the nontrivial interplay between the χ SB and CSC phases induced by the vector interaction is expected to be a universal phenomenon and might give a clue to understanding results obtained with two-color QCD on the lattice.

§1. Introduction

It is one of the central issues in hadron physics to determine the phase diagram of strongly interacting matter in the temperature (T)-chemical potential (μ) or T - ρ_B plane, with ρ_B being the baryonic density. In extremely hot and dense matter, the non-Abelian nature of QCD ensures that the colored quarks and gluons are not confined, and chiral symmetry is restored. Lattice simulations of QCD^{1),2)} show that the QCD vacuum undergoes a chiral and deconfinement transition at a temperature T_c around 150–175 MeV at vanishing chemical potential, with the order and critical temperature being dependent on the number of active flavors. Although there have been several promising attempts^{3)–9)} to make simulations of lattice QCD with finite μ possible, they have still not progressed enough to predict anything definite about the phase transition at finite ρ_B or μ . It is widely believed on the basis of effective theories^{10)–12)} and chiral random matrix theory¹³⁾ that the chiral phase transition from the chiral-symmetry broken to the restored phase is first order at vanishing temperature. Furthermore, people believes now that the critical line of the first order chiral transition continues for smaller chemical potentials in the T - μ plane and ends at some point with $T = T_e$ and $\mu = \mu_e$, which is called the endpoint. We notice that the first-order chiral transition is accompanied by a jump in the baryon density.

Recent renewed interest in color superconductivity (CS)^{14)–22)} has stimulated intensive studies of the QCD phase structure at finite density in the low temperature region, which in turn are revealing a rich phase structure of high density hadron/quark matter with CS.^{23)–29)} Possible relevance of CS to characteristic phenomena observed for neutron stars are being actively discussed.^{30),31)} Some recent studies have also suggested that experiments on the Earth using heavy-ion collisions with large baryon stopping can elucidate something about CS in dense matter.^{32),33)}

The purpose of the present paper is to reveal new characteristics of the chiral to color superconducting (CSC) transition based on a simple effective model incorporating the vector interaction by focusing on the implication of the density jump accompanied by the chiral transition.

Low-energy effective models^{10)–12),23),24)} are useful to study not only the chiral transition but also CS in dense hadronic matter. For example, chiral models of the Nambu-Jona-Lasinio type,³⁴⁾ which can be considered simplified versions of those with an instanton-induced interaction, accurately describe the gross features of the T dependence of the chiral quark condensates of the lightest three quarks as given by lattice QCD, and predict that the chiral transition for $\mu \neq 0$ is rather strongly first order at low temperatures when the vector interaction is absent or small.^{12),35),36)} Chiral effective theories show that the gap Δ of CS

may become as large as 100 MeV in relatively low densities, where a phase change from the chiral symmetry breaking (χ SB) phase to the CSC phase may also occur.^{23),24)}

However, although many works on CS have been carried out with the use of effective models, the vector interaction,^{36)–48)}

$$\mathcal{L}_V = -G_V(\bar{\psi}\gamma^\mu\psi)^2, \quad (1.1)$$

has been scarcely taken into account, with the exception of very recent works.^{47),48)} Our point is that such a vector interaction is chiral invariant and naturally appears in the effective models derived from microscopic theories and, as we shall show, indeed can have strong effects on the chiral-to-CSC transition and the properties of the CSC phase.

Although it may not be a common knowledge in the physics community, the importance of the vector coupling for the chiral transition is known; i.e., the vector coupling weakens the phase transition and moves the chiral restoration to a larger value of μ .^{36),42),46)} This can be intuitively understood as follows.⁴⁹⁾ According to thermodynamics, when two phases I and II are in an equilibrium state, their temperatures $T_{I,II}$, pressures $P_{I,II}$ and the chemical potentials $\mu_{I,II}$ are the same:

$$T_I = T_{II}, \quad P_I = P_{II}, \quad \mu_I = \mu_{II}. \quad (1.2)$$

If I and II are the chirally broken and restored phase with quark masses satisfying $M_I > M_{II}$, the last equality further tells us that the chirally restored phase has a higher density than the broken phase, because $\mu_{I,II}$ at vanishing temperature are given by $\mu_i = \sqrt{M_i^2 + p_{F_i}^2}$, ($i = I, II$), and hence $p_{F_I} < p_{F_{II}}$, where p_{F_i} is the Fermi momentum of the i -th phase. Thus it is seen that chiral restoration at finite density is necessarily accompanied by a density jump to a higher density state with a large Fermi surface, which in turn favors the formation of Cooper instability leading to CS.

However, since the vector coupling includes the term $(\bar{\psi}\gamma^0\psi)^2$, it gives rise to a repulsive energy proportional to the density squared, i.e. $G_V\rho_B^2/2$, which is larger in the restored phase than in the broken phase; the vector coupling weakens and delays the phase transition of the chiral restoration at low temperatures. Thus one expects naturally that \mathcal{L}_V causes the chiral restoration and the formation of CS to shift to higher chemical potentials, and may alter the nature of the transition from the χ SB phase to the CSC phase drastically.

Is it legitimate to include a vector term like (1.1) in an effective Lagrangian? First of all, one should notice that the instanton-anti-instanton molecule model,^{12),24)} as well as the renormalization-group equation,^{50),51)} shows that \mathcal{L}_V appears as a part of the effective interactions together with those in the scalar channels, which are responsible for the chiral symmetry breaking (χ SB): The instanton-anti-instanton molecule model gives for the

effective interaction between quarks

$$\begin{aligned} \mathcal{L}_{molsym} = G_{mol} \{ & \frac{2}{N_c^2} [(\bar{\psi}\tau^a\psi)^2 + (\bar{\psi}\tau^a i\gamma_5\psi)^2] \\ & - \frac{1}{2N_c^2} [(\bar{\psi}\tau^a\gamma_\mu\psi)^2 - (\bar{\psi}\tau^a\gamma_\mu\gamma_5\psi)^2] + \frac{2}{N_c^2}(\bar{\psi}\gamma_\mu\gamma_5\psi)^2 \} + \mathcal{L}_8, \end{aligned} \quad (1.3)$$

where $\tau^a = (\vec{\tau}, 1)$ and \mathcal{L}_8 denotes the color octet part of the interaction, which we shall not write down. Near the phase transition, the instanton molecules are polarized in the temporal direction, Lorenz invariance is broken, and thus the vector interactions are modified as $(\bar{\psi}\gamma_\mu\Gamma\psi)^2 \rightarrow (\bar{\psi}\gamma_0\Gamma\psi)^2$. Notice that the instanton-induced interaction breaks the $U_A(1)$ symmetry. In reality, however, there should also exist $U_A(1)$ -symmetric interactions such as the one-gluon exchange interaction or its low-energy remnant as

$$\mathcal{L}_{LL}^0 = G_u^0 \{ (\bar{\psi}_L\gamma_0\psi_L)^2 - (\bar{\psi}_L\gamma_i\psi_L)^2 \}, \quad (1.4)$$

where ψ_L denotes the left-handed quark field. It is shown using the renormalization group equation that the strengths of the $U_A(1)$ -symmetric and violating effective interactions are of the same order near the Fermi surface. Thus one sees that the vector interaction exists together with other chiral invariant terms which are usually used. Therefore, one may say that the previous works dealing with the χ SB-to-CSC phase transition without incorporating the vector interaction \mathcal{L}_V are all incomplete, because this interaction may alter the nature of the phase transition significantly.

We shall show in this paper that the inclusion of the vector coupling induces a novel interplay between the χ SB and CS through the difference of the respective favoring baryon densities and changes both the nature of the phase transition and the phase structure in the low temperature region drastically ^{*)}. The resultant phase diagram and the behavior of the chiral and diquark condensates as functions of (T, μ) will be found to have a good correspondence with those given in two-color QCD on the lattice.⁸⁾ It is thus found that our simple model gives a possible mechanism underlying the lattice results.

This paper is organized as follows. In the next section, the Lagrangian to be used is introduced. In §3, we shall give the thermodynamic potential and the self-consistency condition for the quark condensate and the pairing field. Numerical results are presented in §4. The final section is devoted to a summary and concluding remarks. The appendix summarizes the effects of the vector interaction on the chiral transition when the CS is not incorporated.

^{*)} Preliminary results have been reported in Ref. 52)

§2. Model

As a chiral effective model which embodies the vector interaction as well as the usual scalar terms driving χ SB, we use a simple Nambu-Jona-Lasinio (NJL) model with two flavors ($N_f = 2$) and three colors ($N_c = 3$), following Ref. 23). The NJL model may be regarded as a simplified version of that with instanton-induced interactions and can also be derived using a Fierz transformation of the one-gluon exchange interaction with heavy-gluon approximation (see 10),11),53)–55)). This effective model has the merit that it can be used to investigate the chiral transition and CS simultaneously, and hence describes their interplay. It was shown⁵⁶⁾ that the physical content given with the instanton model²³⁾ can be nicely reproduced by the simple NJL model with a simple three-momentum cutoff. This means that although there are several choices for the high momentum cutoff which mimics the asymptotic freedom, the magnitude of the gap is largely determined by the strength of the interaction and is insensitive to the form of the momentum cutoff.³⁰⁾ The Lagrangian density thus reads

$$\mathcal{L} = \mathcal{L}_0 + \mathcal{L}_I, \quad (2.1)$$

where

$$\mathcal{L}_0 = \bar{\psi}(i\gamma \cdot \partial - \mathbf{m})\psi, \quad (2.2)$$

with \mathbf{m} being the current quark mass matrix $\mathbf{m} = \text{diag}(m_u, m_d)$, and

$$\mathcal{L}_I = \mathcal{L}_S + \mathcal{L}_V + \mathcal{L}_C, \quad (2.3)$$

with

$$\mathcal{L}_S = G_S \{ (\bar{\psi}\psi)^2 + (\bar{\psi}i\gamma_5\tau\psi)^2 \}, \quad (2.4)$$

and

$$\mathcal{L}_C = G_C \{ (\bar{\psi}i\gamma_5\tau_2\lambda_A\psi^C)(\bar{\psi}^C i\gamma_5\tau_2\lambda_A\psi) + (\bar{\psi}\tau_2\lambda_A\psi^C)(\bar{\psi}^C\tau_2\lambda_A\psi) \}. \quad (2.5)$$

\mathcal{L}_V is given in (1.1). Here, $\psi^C \equiv C\bar{\psi}^T$, with $C = i\gamma^2\gamma^0$ being the charge conjugation operator, and τ_2 and λ_A 's are the second component of the Pauli matrix representing the flavor $SU(2)_f$, and the antisymmetric Gell-Mann matrices representing the color $SU(3)_c$, respectively. The scalar coupling constant $G_S = 5.5 \text{ GeV}^{-2}$ and the three momentum cutoff $\Lambda = 631 \text{ MeV}$ are chosen so as to reproduce the pion mass $m_\pi = 139 \text{ MeV}$ and the pion decay constant $f_\pi = 93 \text{ MeV}$ with the current quark mass $m_u = m_d = 5.5 \text{ MeV}$;¹¹⁾ we have assumed isospin symmetry. It should be noted that the existence of the diquark coupling G_C

and the vector coupling G_V do not affect the determination of the pion decay constant and the chiral condensate. Although, there are several sources to determine the diquark coupling such as the diquark-quark picture of baryons,^{53)-55),57)} the instanton-induced interaction,²⁴⁾ renormalization group analysis,^{50),51)} and so on, we shall take $G_C/G_S = 0.6$, which accurately reproduces the phase diagram obtained with the instanton-induced interaction.²³⁾ As for the vector coupling, we vary it as a free parameter in the range of $G_V/G_S = 0 - 0.5$ to see the effect of the vector coupling on the phase diagram. We remark that the vector coupling G_V is given by $0.25G_S$ in the instanton-anti-instanton molecule model¹⁸⁾ and $0.5G_C$ in the renormalization-group analysis;^{50),51)} the range we employ for G_V thus encompasses these *physical* values.

§3. Thermodynamic Potential and Gap Equations

In this section, we calculate the thermodynamic potential in the mean-field approximation and derive the coupled gap equations for the chiral and diquark condensates.

The thermodynamic potential Ω is defined by

$$\Omega = -T \ln \text{Tr} e^{-\beta \hat{K}}, \quad (3.1)$$

where $\beta = 1/T$ is the inverse temperature and $\hat{K} = \hat{H} - \mu \hat{N}$, with \hat{H} and \hat{N} being the Hamiltonian and the quark number operator, respectively. The expectation value of the quark number is given by

$$N_q = \langle \hat{N} \rangle, \quad (3.2)$$

where

$$\langle \hat{O} \rangle = \text{Tr} e^{-\beta(\hat{K}-\Omega)} \hat{O} \quad (3.3)$$

denotes the statistical average of \hat{O} . The quark number density is given by

$$\rho_q = N_q/V = \langle \bar{\psi} \gamma^0 \psi \rangle, \quad (3.4)$$

where V denotes the volume of the system, and it is assumed that the vacuum contribution to the quark number is subtracted.^{58) *)}

The quark number N_q can be calculated by means of a thermodynamic relation from Ω as $N_q = -\partial\Omega/\partial\mu$, and accordingly, ρ_q is obtained from the thermodynamic potential density

*) The rotational invariance of the system, which we assume, implies that the spatial component of the expectation value $\langle \bar{\psi} \gamma^i \psi \rangle$ vanishes.

as^{*)}

$$\rho_q = -\frac{\partial(\Omega/V)}{\partial\mu}. \quad (3.5)$$

Since quarks have baryon number 1/3, the baryon number density and chemical potential are given by $\rho_B = 1/3 \cdot \rho_q$ and $\mu_B = 3\mu$, respectively, where iso-spin symmetry is assumed. We shall use the quark number density ρ_q and chemical potential μ for the formulation, but ρ_B and μ_B will be used in the presentation of the numerical results in §4.

To apply the mean-field approximation (MFA), we first assume that the system has a quark-antiquark condensate $\langle\bar{\psi}\psi\rangle$ and a diquark condensate $\langle\bar{\psi}^C i\gamma_5\tau_2\lambda_2\psi\rangle$, where λ_A is restricted to λ_2 owing to the color $SU(3)_c$ symmetry. In the MFA, \hat{K} is replaced by

$$\begin{aligned} \hat{K}_{\text{MFA}} = & \int d^3\mathbf{x} \left[\bar{\psi}[-i\vec{\gamma} \cdot \vec{\nabla} + (m + M_D) - (\mu - 2G_V\rho_q)\gamma_0]\psi + \frac{1}{2}(\Delta^*\bar{\psi}^C i\gamma_5\tau_2\lambda_2\psi + \text{h. c.}) \right. \\ & \left. + \frac{M_D^2}{4G_S} + \frac{|\Delta|^2}{4G_C} - G_V\rho_q^2 \right]. \end{aligned} \quad (3.6)$$

Here, M_D and Δ give the dynamically generated quark mass and the gap due to the CS, respectively:

$$M_D = -2G_S\langle\bar{\psi}\psi\rangle, \quad \Delta = -2G_C\langle\bar{\psi}^C i\gamma_5\tau_2\lambda_2\psi\rangle. \quad (3.7)$$

We notice here that μ in \hat{K}_{MFA} appears in the combination

$$\mu - 2G_V\rho_q \equiv \tilde{\mu}. \quad (3.8)$$

Thus, the thermodynamic potential Ω_{MFA} in MFA per unit volume is calculated to be

$$\begin{aligned} \omega(M_D, \Delta; T, \mu) & \equiv \Omega_{\text{MFA}}/V \\ & = \frac{M_D^2}{4G_S} + \frac{|\Delta|^2}{4G_C} - G_V\rho_q^2 \\ & \quad - 4 \int \frac{d^3p}{(2\pi)^3} \left\{ E_{\mathbf{p}} + T \log(1 + e^{-\beta\xi_-}) (1 + e^{-\beta\xi_+}) \right. \\ & \quad \left. + \text{sgn}(\xi_-) \epsilon_- + \epsilon_+ + 2T \log(1 + e^{-\text{sgn}(\xi_-)\beta\epsilon_-}) (1 + e^{-\beta\epsilon_+}) \right\}, \end{aligned} \quad (3.9)$$

where $E_p = \sqrt{p^2 + M^2}$, $\xi_{\pm} = E_p \pm \tilde{\mu}$ and $\epsilon_{\pm} = \sqrt{\xi_{\pm}^2 + |\Delta|^2}$, with

$$M = m + M_D \quad (3.10)$$

^{*)} This is a familiar procedure in the σ - ω model.⁵⁹⁾

being the total (constituent) quark mass and $sgn(\xi_-)$ the sign function. Our thermodynamic potential reduces to those given in Refs. (23), (56) when $G_V = 0$. The quark density ρ_q appearing in (3.9) is expressed as a function of the condensates (M_D, Δ) through the thermodynamical relation (3.5) as

$$\rho_q = 4 \int \frac{d^3p}{(2\pi)^3} \left\{ n(\xi_-) - n(\xi_+) - \frac{\xi_-}{\epsilon_-} \tanh \frac{\beta\epsilon_-}{2} + \frac{\xi_+}{\epsilon_+} \tanh \frac{\beta\epsilon_-}{2} \right\}, \quad (3.11)$$

where $n(\xi_{\pm})$ is the Fermi distribution function: $n(\xi_{\pm}) = 1/(\exp\{\beta\xi_{\pm} + 1\})$. Equation (3.9) together with Eq.(3.11) gives the thermodynamic potential ω with the condensates (M_D, Δ) being the variational parameters at given (T, μ) ; their optimal values give the absolute minimum of ω .

The chiral and diquark condensates in the equilibrium state at given (T, μ) should satisfy the stationary conditions for the thermodynamic potential,

$$\left. \frac{\partial\omega}{\partial M_D} \right|_{\Delta} = 0, \quad \left. \frac{\partial\omega}{\partial \Delta} \right|_{M_D} = 0, \quad (3.12)$$

which are reduced to the self-consistency conditions for the two condensates,

$$M_D = 8G_S M \int \frac{d^3p}{(2\pi)^3} \frac{1}{E_p} \left\{ 1 - n(\xi_-) - n(\xi_+) + \frac{\xi_-}{\epsilon_-} \tanh \frac{\beta\epsilon_-}{2} + \frac{\xi_+}{\epsilon_+} \tanh \frac{\beta\epsilon_+}{2} \right\}, \quad (3.13)$$

$$\Delta = 8G_C \Delta \int \frac{d^3p}{(2\pi)^3} \left\{ \frac{1}{\epsilon_-} \tanh \frac{\beta\epsilon_-}{2} + \frac{1}{\epsilon_+} \tanh \frac{\beta\epsilon_+}{2} \right\}. \quad (3.14)$$

Here we have utilized the chain rule

$$\left. \frac{\partial\omega}{\partial M_D} \right|_{\Delta} = \left. \frac{\partial\omega}{\partial M_D} \right|_{\Delta, \rho_q} + \left. \frac{\partial\rho_q}{\partial M_D} \right|_{\Delta} \cdot \left. \frac{\partial\omega}{\partial\rho_q} \right|_{M_D, \Delta}, \quad (3.15)$$

and that for the Δ -derivative, together with the fact that Eq. (3.11) ensures the relation

$$\left. \frac{\partial\omega}{\partial\rho_q} \right|_{M_D, \Delta} = 0. \quad (3.16)$$

In analogy to the BCS theory of the superconductivity, we call Eqs. (3.13) and (3.14) the gap equations. Notice, however, that a solution of the gap equations may only give a *local* minimum, or even *maximum* of the thermodynamic potential, and it is only a candidate of the optimal value of the condensates; one must check whether it gives the absolute minimum of the thermodynamic potential.

From the structure of the coupled gap equations and the thermodynamic relation (3.11) for ρ_q , one can extract some interesting properties of the condensates (M_D, Δ) as functions of (T, μ) and also of (T, ρ_q) .

(1) Once the absolute minimum of the thermodynamic potential and, accordingly, the optimal value of (M_D, Δ) are found at given (T, μ) , the quark density ρ_q is given by Eq. (3.11). The coupled gap equations (3.13) and (3.14) show us that the optimal value of (M_D, Δ) is a function of T and $\tilde{\mu}$, and in this way the possible G_V dependence is absorbed into $\tilde{\mu}$. Furthermore, if $(M_D(T, \mu), \Delta(T, \mu))$ is a solution of the coupled gap equations with $G_V = 0$, then

$$(M_D(T, \tilde{\mu}), \Delta(T, \tilde{\mu})) \equiv (M_D(T, \mu - 2G_V\rho_q), \Delta(T, \mu - 2G_V\rho_q)) \quad (3.17)$$

is a solution with $G_V \neq 0$. Thus, the whole solution as a function of μ is shifted toward larger μ by an amount $2G_V\rho_q$.

(2) Next, we shall examine how the solutions of the coupled gap equations behave as functions of (T, ρ_q) instead of (T, μ) . Let the 0-th order approximation of the condensates be given. Then Eq. (3.11) gives $\tilde{\mu}$ as a function of (T, ρ_q) , i.e., $\tilde{\mu} = \tilde{\mu}(T, \rho_q)$. Thus, the first-order approximation of the condensates (M_D, Δ) is given as the solution to the coupled gap equations (3.13) and (3.14), which are only dependent on T and $\tilde{\mu}$, not on μ and ρ_q , separately; possible G_V dependence is absorbed into $\tilde{\mu}(T, \rho_q)$. Thus, repeating this procedure, one sees that (M_D, Δ) becomes only a function of T and ρ_q and is independent of G_V , because $\tilde{\mu}$, through which G_V can affect the formulas, actually only plays the role of a dummy variable. Thus we have proved that there is no effect of the vector interaction on the behavior of the solution to the coupled gap equation as functions of (T, ρ_q) .

(3) Does it mean that there is no trace of the presence of the vector interaction in the phase diagram in the T - ρ plane? The answer is no. The effect of the vector interaction manifests itself in the critical point or line when the transition is first order. In this case, there are several solutions to the coupled gap equations (3.13) and (3.14), corresponding to the local minima, maxima and even saddle points of ω ; notice that these solutions correspond to different baryon densities. Since the thermodynamic potential (3.9) is explicitly dependent on G_V in a combination with the quark density, the relative magnitudes of the local minima change and can be altered with the vector interaction: In Fig. 1, the right (left) figure in the upper panel shows the contour map of the thermodynamic potential $\omega(M_D, \Delta)$ with $G_V/G_S = 0.2$ ($G_V/G_S = 0$) at $T = 0$ and $\mu_B = \mu_{B0} = 1035$ MeV, which is actually found to be the critical point. The thermodynamic potential $\omega(M_D, \Delta)$ as a function of M_D at given $\Delta = 0, 25, 50$ and 80 MeV; i.e., the cross sections along the lines shown in the upper panels are given in the lower panels, where the solid (dashed) lines denote ω with $G_V/G_S = 0.2$ ($G_V/G_S = 0$). One clearly sees that the vector interaction increases the thermodynamic potential in the small M_D region for every Δ ; notice that the system with smaller M_D is at higher density, as discussed in §1. Thus the absolute minimum given with $\Delta \sim 50$ MeV

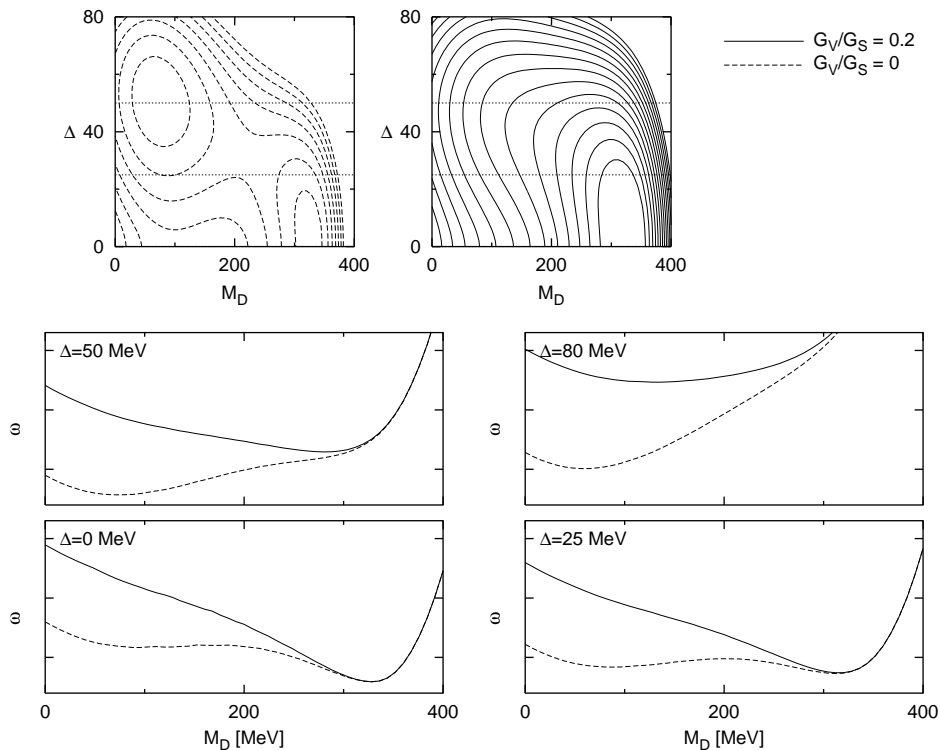


Fig. 1. The upper panels show contour maps of the thermodynamic potential ω at $(T, \mu_B) = (0, 1035)$ MeV with $G_V/G_S = 0$ (left panel) and $G_V/G_S = 0.2$ (right panel) in the M_D - Δ plane. The difference between the values of ω for the adjacent contour lines is 7.5×10^6 MeV⁴. The lower four panels are cross sections of ω cut in a plane with Δ fixed at 0, 25, 50 and 80 MeV. The solid (dashed) lines represent the $G_V/G_S = 0.2$ ($G_V/G_S = 0$) case.

at small M_D when $G_V = 0$ ceases to be even a local minimum with finite G_V/G_S , and the local minimum at $M_D \sim 300$ MeV with $\Delta \sim 0$ in turn becomes the unique local, and hence, the absolute minimum. Thereby the double-minimum structure disappears, and the first order transition is altered to a crossover. In short, the critical temperatures and densities at which the transition from one local minimum to the other occurs are strongly affected by the vector interaction, and the critical line of the first-order transition in the T - ρ_q plane is changed with the vector interaction.

In passing, we remark that ρ_q cannot be interpreted as a variational parameter with which the thermodynamic potential is minimized: Since Eq. (3.11) is obtained by the stationary condition Eq. (3.16), one might have imagined that the equilibrium state could be determined by searching for the minimum point of the thermodynamic potential with ρ_q being a variational parameter together with M_D and Δ .⁴⁷⁾ However, Eq. (3.16) is found to give a local *maximum* of the thermodynamic potential. That is, the absolute minimum of the thermodynamic potential in the M - Δ - ρ_q space, if it exists, does not give the thermodynamical

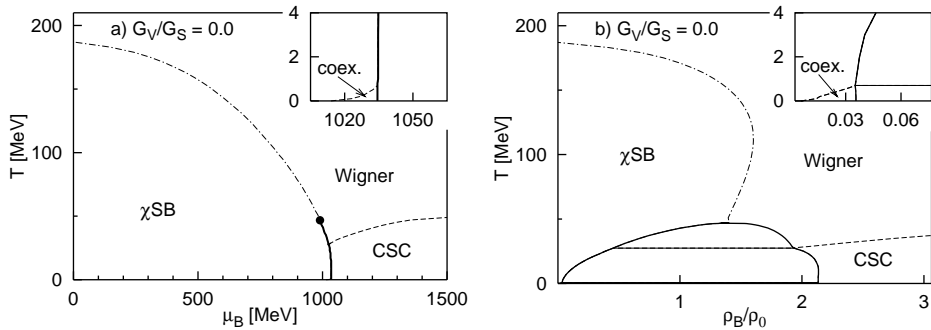


Fig. 2. (a) The phase diagram in the T - μ_B plane with $G_V = 0$. There are four phases; the χ SB, CSC, Wigner, and coexisting phases. The small panel is an enlargement around the border of the χ SB and CSC phases at $T = 0$. The solid line represents the critical line of a first-order phase transition, the dashed line a second-order phase transition, and the dot-dashed line a crossover. (b) The corresponding phase diagram in the T - ρ_B plane in units of the nuclear matter density ρ_0 . There exist mixed phases corresponding to the first-order transitions seen in (a).

equilibrium state.

§4. Numerical results and discussion

In this section, we show the numerical results and discuss the effects of the vector coupling on the phase diagram, the T - μ_B and T - ρ_B dependence of the order parameters.

4.1. Phase diagram with no vector interaction

As preliminary to the discussion on the effects of the vector interaction, we first present the phase structure without the vector interaction. We shall show that a coexisting phase appears where the quarks with dynamically generated mass are color superconducting. This is a manifestation of competition between the χ SB and CSC phase transition.

In Fig. 2(a), the phase diagram in the T - μ plane is shown. One can see that there are four different phases, i.e. the χ SB phase, the normal quark phase, which we call the Wigner phase, the CSC phase, and a “coexisting” phase of χ SB and CS; as seen from the upper small panel, which is an enlargement of the part around the solid line near zero temperature, the last phase, in which quarks with dynamically generated mass are color superconducting, occupies only a small region in the T - μ plane near zero temperature with μ slightly smaller than $\mu_{B0} = 1035$ MeV.

In the figure, the critical line of first- and second-order transitions are represented by the solid and dashed lines, respectively; notice that there exists a dashed line in the upper small panel. We remark that there are three kinds of first-order transitions: χ SB-Wigner,

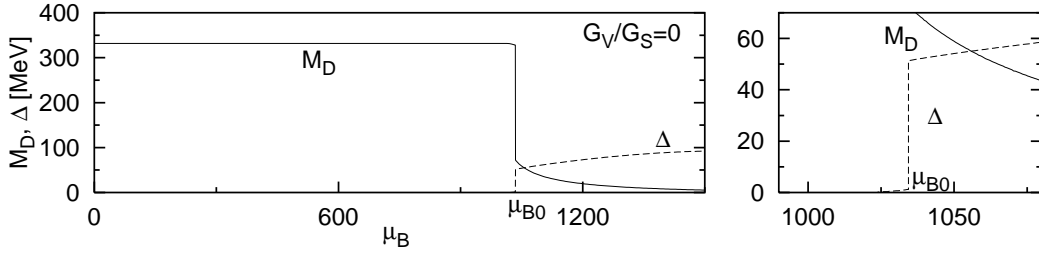


Fig. 3. The order parameters M_D and Δ at $T = 0$ as functions of μ_B with $G_V = 0$. There are discontinuities of the order parameters at $\mu_{B0} = 1035$ MeV. An enlarged figure near the critical point is also shown. The gap Δ is finite even in the region $\mu_B < \mu_{B0}$.

χ SB-CSC and coexisting-CSC transitions. An artificial critical line of the crossover chiral transition is also shown by the dash-dotted line on which the dynamical quark mass takes the same value as that at the endpoint $M_D = 186$ MeV, so that the crossover critical line is connected continuously with the critical line of the first-order transition at the endpoint.

*) With this definition of the critical line for the crossover chiral transition, the critical temperature at vanishing chemical potential ($\mu = 0$) is found to be 187 MeV, which is slightly larger than the critical temperature obtained in simulations of lattice QCD with two flavors.²⁾

In accordance with a widely accepted view,^{30),31)} one sees that the chiral transition is first-order at low temperatures: The critical line of the first-order transition emerging from a point in the zero-temperature line terminates at

$$(T_e, \mu_{Be}) = (47, 990) \text{ MeV.}$$

The figure also shows that the phase transition from the CSC to the Wigner phase is second order when T is raised in our model, in which the gluon fields are not explicitly included.¹⁵⁾ We have found that the χ SB phase is transformed into the coexisting phase at very low temperatures by a second-order transition when μ is raised, as shown in the small panel.

To see more detail of the coexisting phase, we show the μ dependence of M_D and Δ at $T = 0$ in Fig. 3. One can see that M_D (Δ) shows a discontinuous decrease (increase) at $\mu_B = \mu_{B0}$, which clearly indicates a first-order chiral (CSC) transition at this point. A notable point here is that M_D has a finite value even in the CSC phase, because of the finite current quark mass; notice that M_D is proportional to the chiral condensate and not the total (constituent) quark mass $M = m + M_D$. Although we do not show the result here, we have checked that M_D vanishes in the CSC phase in the chiral limit (nevertheless see Fig. 7 for $G_V/G_S = 0.2$). On the other hand, there is a region in which Δ becomes finite

*) We have followed the criterion used in Ref. 36).

in the χ SB phase, which remains the case in the chiral limit. We have called this phase the coexisting phase.

We notice that a coexisting phase similar to ours was obtained in some previous works.^{24),60)–63)}

*) For example, Rapp et al.²⁴⁾ showed that the instanton-anti-instanton molecule model admits such a coexisting phase at finite chemical potential, although the phase structure at $T \neq 0$ was not examined. However, they questioned the robustness of the existence of the coexisting phase, because other calculations using a similar NJL-type chiral model,²³⁾ in which the effective scalar coupling constant G_S in our notation is relatively large, did not exhibit such a coexisting phase. In fact, we have also checked that if a slightly larger G_S is used, the coexisting phase disappears even in our case. We shall show, however, that the vector interaction induces a competition between the χ SB and CSC phase transition, and thereby the existence of the coexisting phase always becomes possible with a sufficiently large vector coupling. **)

The phase diagram in the T - ρ_B plane is shown in Fig. 2(b). This phase structure is schematically presented in Fig. 4. Corresponding to the three types of first-order transitions mentioned above, there exist three mixed phases, which we call I, II and III, respectively: I is a mixed phase of the χ SB and Wigner phases, while II and III are mixed phases of the χ SB and CSC phases, and the coexisting and CSC phases, respectively. We remark that various other mixed phases are possible when the CSC phase is incorporated than when it is not.

This ends our investigation of the phase structure without the vector interaction. When the vector interaction is included, the phase structure may be changed significantly, which we shall show is indeed the case in the next subsection.

4.2. Phase structure with the vector interaction

In this subsection, we discuss effects of the vector interaction on the phase structure of hot and dense quark matter by varying the vector coupling G_V by hand in the range of $G_V/G_S = 0 - 0.5$. One will see that the vector interaction causes a nontrivial interplay between the χ SB and CS phase, causing the optimal condensates to greatly fluctuate in a combined way. This effect was not elucidated in the previous work.⁴⁸⁾

The phase structure in the T - μ plane with $G_V/G_S = 0.2$ is shown in Fig. 5(a). The phase diagram consists of the χ SB, Wigner, CSC and coexisting phases, as in Fig. 2(a).

*) In Ref. 56), the full coupled gap equations for M_D and Δ were not solved, which is necessary to find the coexisting phase. The coexisting phase discussed in Ref. 64) using the NJL model is thermally unstable.

**) We remark that if the ratio G_C/G_S in our notation is artificially large, the coexisting phase can be also realized in a broad region in the T - μ plane, as shown in the random matrix model⁶²⁾ and in the NJL model.⁶³⁾

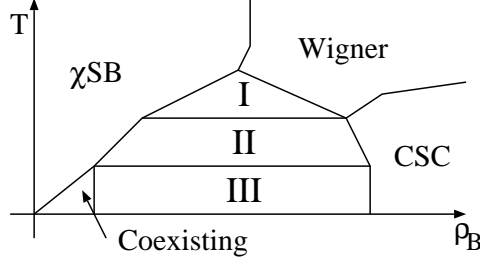


Fig. 4. A schematic figure accounting for Fig. 2(b). There are three mixed phases in the T - ρ_B plane: I is a mixed phase of the χ SB and Wigner phases, while II and III are mixed phases of the χ SB and CSC phases, and the coexisting and CSC phases, respectively.

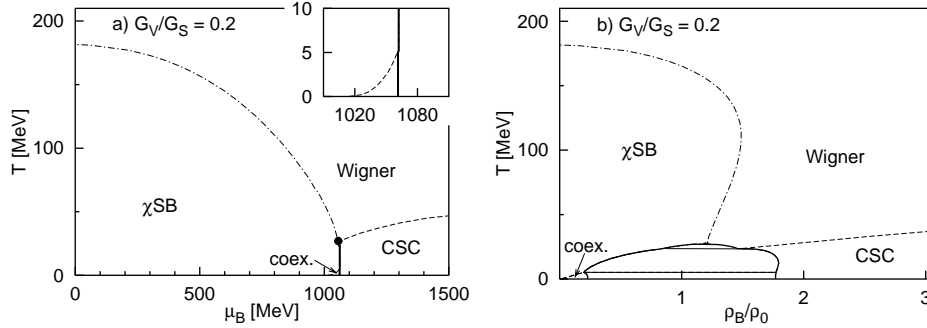


Fig. 5. The phase diagrams with $G_V/G_S = 0.2$ in the T - μ plane (a) and T - ρ plane (b). The solid line represents the critical line of a first-order phase transition, the dashed line a second-order transition and the dot-dashed line a crossover.

The dash-dotted line is the contour line at $M_D = 198$ MeV and is supposed to denote the critical line of the crossover transition; the solid and dashed lines represent the critical lines of the first-order and second-order transitions, respectively, as in Fig. 2(a). The corresponding phase diagram in the T - ρ plane has the three mixed phases I, II and III which are seen in Fig. 4, as well as the χ SB, Wigner and CSC phases.

From these figures, the following points are notable:

- (1) The endpoint of the first-order transition moves toward a lower temperature and higher chemical potential,

$$(T_e, \mu_{Be}) = (27, 1056) \text{ MeV.}$$

- (2) The chiral restoration is moved toward larger μ . This is because the gap equations (3.13) and (3.14) are functions of T and $\tilde{\mu}$, and thus the explicit G_V dependence is absorbed into $\tilde{\mu}$, as shown in Eq. (3.17). This means that μ given by a fixed M_D is shifted toward larger values as G_V is increased.

- (3) The region of the coexisting phase becomes broader in both T and μ directions in the

T - μ plane, and hence also in the T - ρ plane. This feature is determined dominantly by the behavior of M_D in the χ SB phase. As an example, M_D together with Δ , as a function of μ_B at $T = 0$ is shown in Fig. 6; the same quantities in the chiral limit are shown in Fig. 7. One sees that there appears a small region of μ_B , smaller than but near μ_{B0} in which M_D (Δ) shows a gradual decrease (increase); accordingly, finite M_D and Δ coexist in this region. One should notice here that although the coexistence in this sense is realized even when $\mu_B > \mu_{B0}$, as seen in Fig. 6, M_D in the chiral limit vanishes identically in this region, while the coexistence of M_D and Δ remains for at $\mu_B < \mu_{B0}$ as seen in Fig. 7. In fact, this is also the case when $G_V = 0$, as was noted in §4.1. Thus, calling this the “phase coexisting” makes sense. Anyway, the gradual change of the order parameters means that the first-order transition is weakened. The decrease of M_D also implies that of the total quark mass M , leading to a growth of the Fermi surface for a given μ_q . The larger the Fermi surface, the larger the gap Δ , owing to the BCS mechanism. Thus the region of the coexisting phase in the T - μ_B plane becomes broader. This feature can be applied to the case for $T \neq 0$. In short, the vector interaction promotes the formation of the coexisting phase. This is one of the points which Buballa et al.⁴⁸⁾ did not clarified, because they used a fixed vector coupling.

*) It would be interesting to explore the possible correlation between the appearance of the coexisting phase and the strength of the effective vector coupling extracted, say, from the baryon-number susceptibility,^{44),66),67)} as was done in Ref. 68).

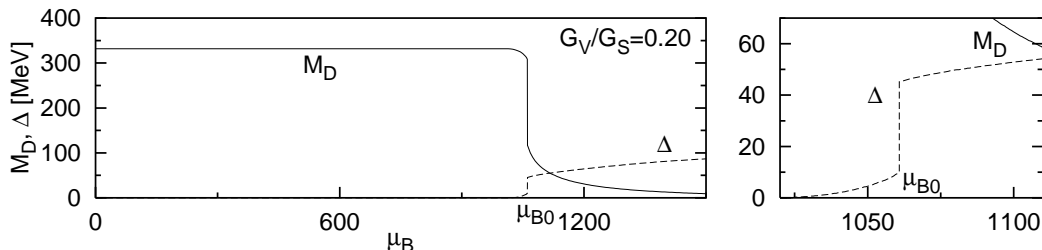


Fig. 6. The order parameters M_D and Δ as a function of μ at $T = 0$ with $G_V/G_S = 0.2$.

The characteristics (1) and (2) of the effects of the vector interaction have been known to exist for the chiral transition without the CSC transition incorporated.^{36),42),46)} (An account of the phase structure without the CSC transition is presented in Appendix A as a reference.)

However, when the interplay between the χ SB and CS phases enhanced with the vector

*) The coexisting phase does not appear in Ref. 48), although a relatively large ratio $G_V/G_S = 0.5$ in our notation is adopted. However, we should also notice that a larger G_S leading to a larger constituent quark mass M than ours is used there. This suggests that if the driving force responsible for the χ SB phase as represented by G_S is strong, a larger ratio G_V/G_S is needed for the realization of the coexisting phase. It is worth mentioning in this respect that the coexisting phase is obtained in the two-color QCD on the lattice in a robust way.⁸⁾

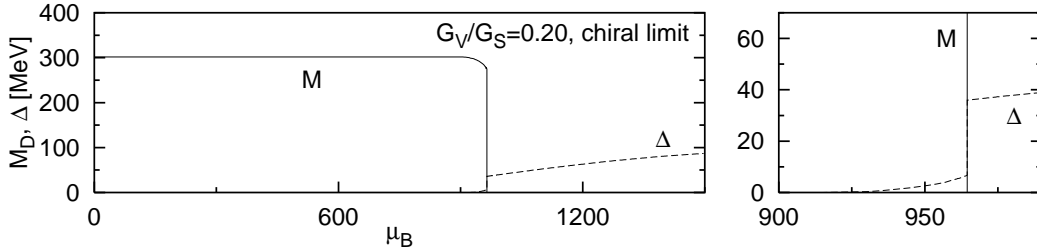


Fig. 7. The order parameters M_D and Δ as functions of μ_B at $T = 0$ in the chiral limit with $G_V/G_S = 0.2$. The other parameters are slightly changed so as to reproduce the physical quantities in the chiral limit: $G_S = 5.01 \text{ GeV}^{-2}$, $\Lambda = 650 \text{ MeV}$ and $G_C = 3.11 \text{ GeV}^{-2}$. One can see that the chiral condensate vanishes completely in the CSC phase while it has a finite value in the coexisting phase. Thus the phase transition from and to the coexisting phase can be unambiguously defined.

interaction is taken into account, the variation of the phase diagram becomes not so simple for larger G_V . In Fig. 8(a), we show the phase diagram in the T - μ plane with $G_V/G_S = 0.35$. It is noteworthy that there appear two endpoints at both sides of the critical line of the first-order transition. Accordingly, the coexisting-CSC transition at low temperatures becomes a crossover transition. We have checked that the crossover transition becomes second order in the chiral limit, and hence a tricritical point appears instead of the endpoint of the first-order transition. As far as we know, this is the first time it has been shown that the critical line of the first-order transition for the chiral restoration can have another endpoint on the low temperature side, implying that the transition from the χ SB phase to the CSC phase at low temperatures becomes a crossover (second order in the chiral limit). Nevertheless it is noteworthy that the two-color QCD on the lattice at nonzero temperature and chemical potential gives a similar phase diagram; see Fig. 1 of Ref. 8). Again, the lattice result might be interpreted in terms of the effective vector coupling, which deserves exploration for the purpose of understanding the underlying physics. The two-endpoint structure does not appear in the random matrix model with two colors,⁶⁵⁾ in which, however, only the two auxiliary fields $\sigma \sim \langle \bar{\psi}\psi \rangle$ and $\Delta \sim \langle \psi C i \gamma_5 \tau_2 \tau_2 \psi \rangle$ are explicitly introduced, but not with the vector field. It would be intriguing to study whether such a phase structure can be realized in the random matrix model with the incorporation of the vector field as an auxiliary field.

The corresponding phase diagram in the T - ρ plane is shown in Fig. 8(b). Its schematic phase structure is represented in Fig. 9. The phases II and III correspond to the mixed phases of the χ SB and CSC phases, and the coexisting and CSC phases, respectively as in Fig. 4. Notably, the phase I does not exist anymore.

To examine the mechanism of the appearance of the two end points in detail, we show the thermodynamic potentials in the M_D - Δ plane for various T and μ in Fig. 10. In the

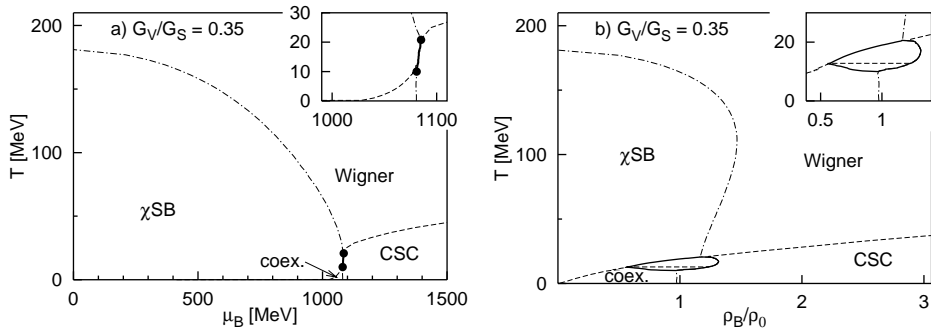


Fig. 8. The phase diagram with $G_V/G_S = 0.35$ in the T - μ plane (a) and T - ρ plane (b). There appear two endpoints of the first-order transition.

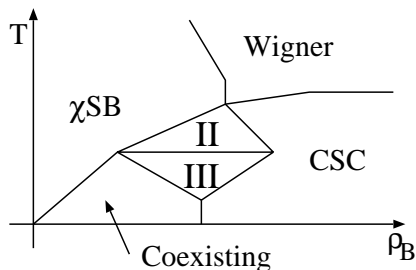


Fig. 9. A schematic figure accounting for Fig. 8(b). The mixed phase I of the χ SB and Wigner phases does not exist in this case.

lowest panels, the thermodynamic potential at $T = 5$ MeV is shown: We see only one local, and hence, the absolute minimum point, which varies continuously as μ is increased. This implies that the phase transition is a crossover at $T = 5$ MeV. At higher temperatures, however, the thermodynamic potential comes to have two local minima near the critical point, as shown in the second and third row panels for $T = 12$ MeV and $T = 15$ MeV, respectively, and the phase transition becomes first order. At even higher temperatures, the double-minimum structure ceases to exist and the thermodynamic potential has only one local minimum again, as shown in the uppermost panel for $T = 22$ MeV, and the phase transition again becomes a crossover.

In our model calculation, the two-end-point structure of the phase diagram appears for finite G_V but in a narrow range of G_V/G_S , i.e. $0.33 \lesssim G_V/G_S \lesssim 0.38$. We should also note that even when the phase transition is first order, the height of the bump between the two local minima of the thermodynamic potential *per particle* is so small that it is found to be comparable with or smaller than the temperature. This means that thermal fluctuations, which are ignored in the mean-field approximation employed in this work, may easily destroy the two-end-point structure. What we have found is that the inclusion of the vector interaction makes the minimum of the thermodynamic potential shallow in the M_D - Δ

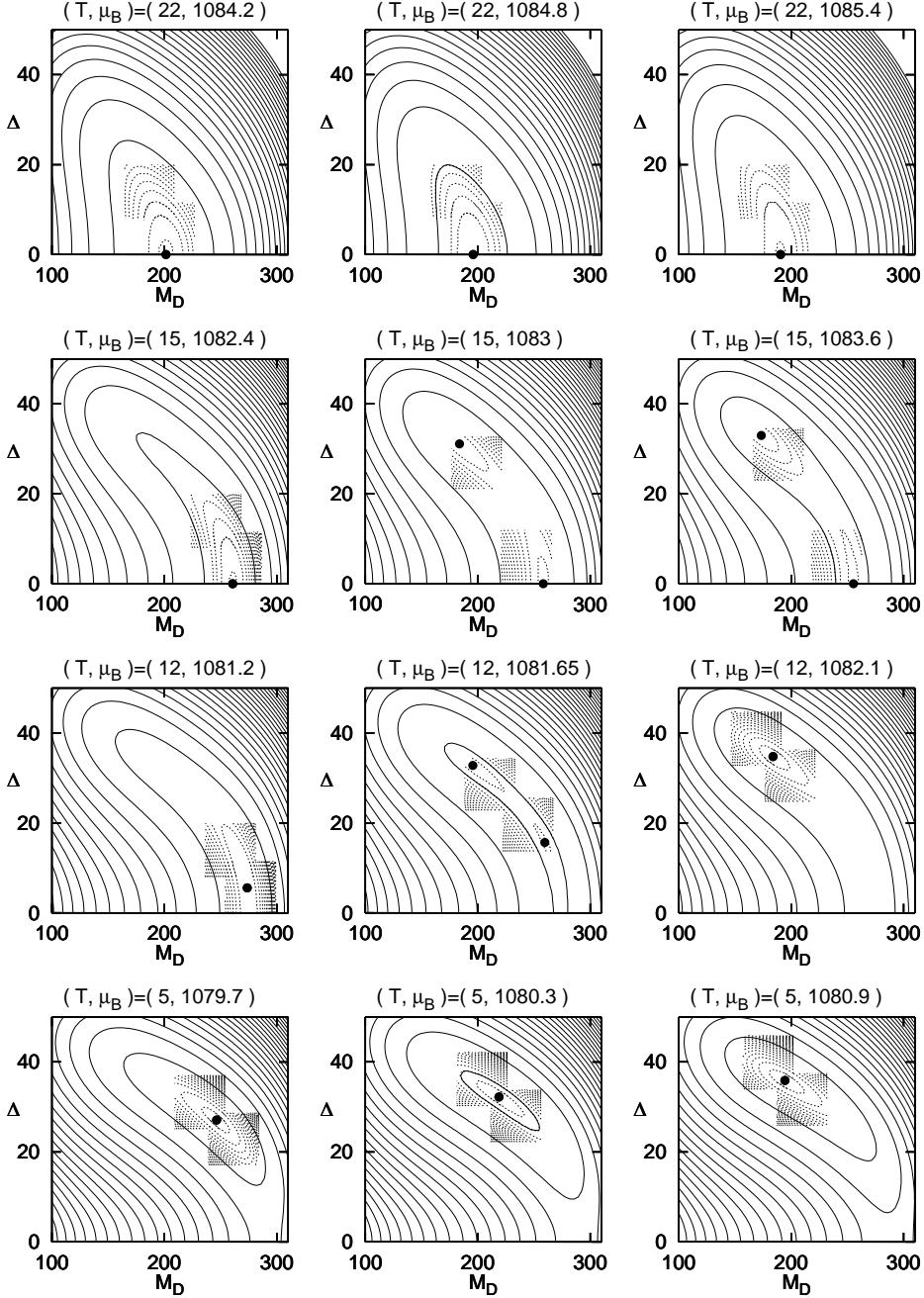


Fig. 10. The contour of the thermodynamic potential in the M_D - Δ plane for various values of (T, μ_B) around the critical point of the first-order transition. The difference between the values of ω for adjacent solid lines is $1.5 \times 10^6 \text{ MeV}^4$. As shown in the second and third row panels, there appear two local minima at $T = 12 \text{ MeV}$ and $T = 15 \text{ MeV}$ with μ_B near the critical value, which indicates that the phase transition is first order at these temperatures. On the other hand, as shown in the bottom and top panels, there always exists only one local, and hence, the absolute minimum at $T = 5$ and 22 MeV , which minimum moves continuously as μ_B is increased, implying that the phase transition is a crossover.

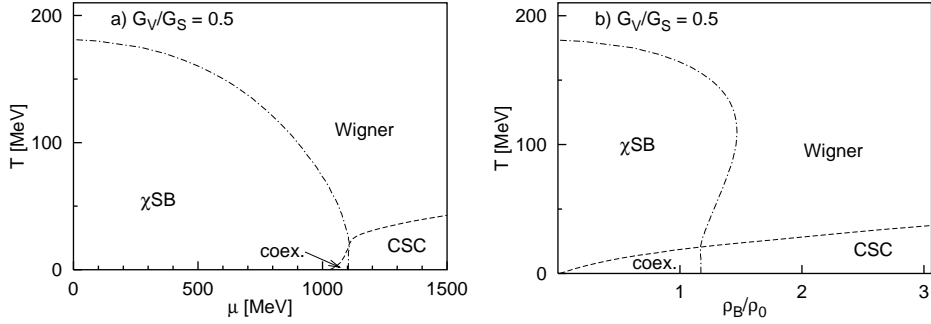


Fig. 11. (a) The phase diagram in the T - μ plane with $G_V/V_S = 0.5$. (b) The corresponding phase diagram in the T - ρ plane.

plane, suggesting the significance of fluctuations of the chiral and diquark condensates in a combined manner. The incorporation of the thermal fluctuations is beyond the scope of this work.

When we consider a larger value of G_V than $0.38G_S$, the first-order transition disappears and it is changed completely into a crossover transition. Figure 11(a) shows the phase diagram in the T - μ plane with $G_V/G_S = 0.5$ as a typical example in this case. The dashed line denotes the second-order transition. The dash-dotted line represents an artificial crossover line on which $M_D = 200$ MeV. The corresponding phase diagram in the T - ρ plane is shown in Fig. 11(b). One can see that there is no first-order transition, and hence no mixed phase. As pointed out in §3, the vector interaction affects the phase diagram in the T - ρ plane only when there is a first-order transition. Therefore, the phase structure in Fig. 11 no longer changes after G_V/G_S exceeds 0.38.

As a nice summary of the effects of the vector interaction on the phase structure of hot and/or dense quark matter, we show three-dimensional plots of the dynamical quark mass M_D and the gap Δ in the T - μ and T - ρ plane in Fig. 12. The thick line represents the critical line of the first-order transition. The dotted points indicate the endpoints. One sees that M_D decreases more smoothly for larger G_V in the T - μ plane. It is clear that the G_V dependence of M_D and Δ in the T - ρ plane appears only in the critical region of the first-order transition.

§5. Summary and concluding remarks

We have investigated effects of the vector coupling on the chiral and color superconducting phase transitions at finite density and temperature in a simple Nambu-Jona-Lasinio model by focusing on the implication of the density jump accompanied by the chiral transition. We have shown that the phase structure is strongly affected by the vector interaction, especially near the critical line between the chiral symmetry breaking (χ SB) and color superconducting

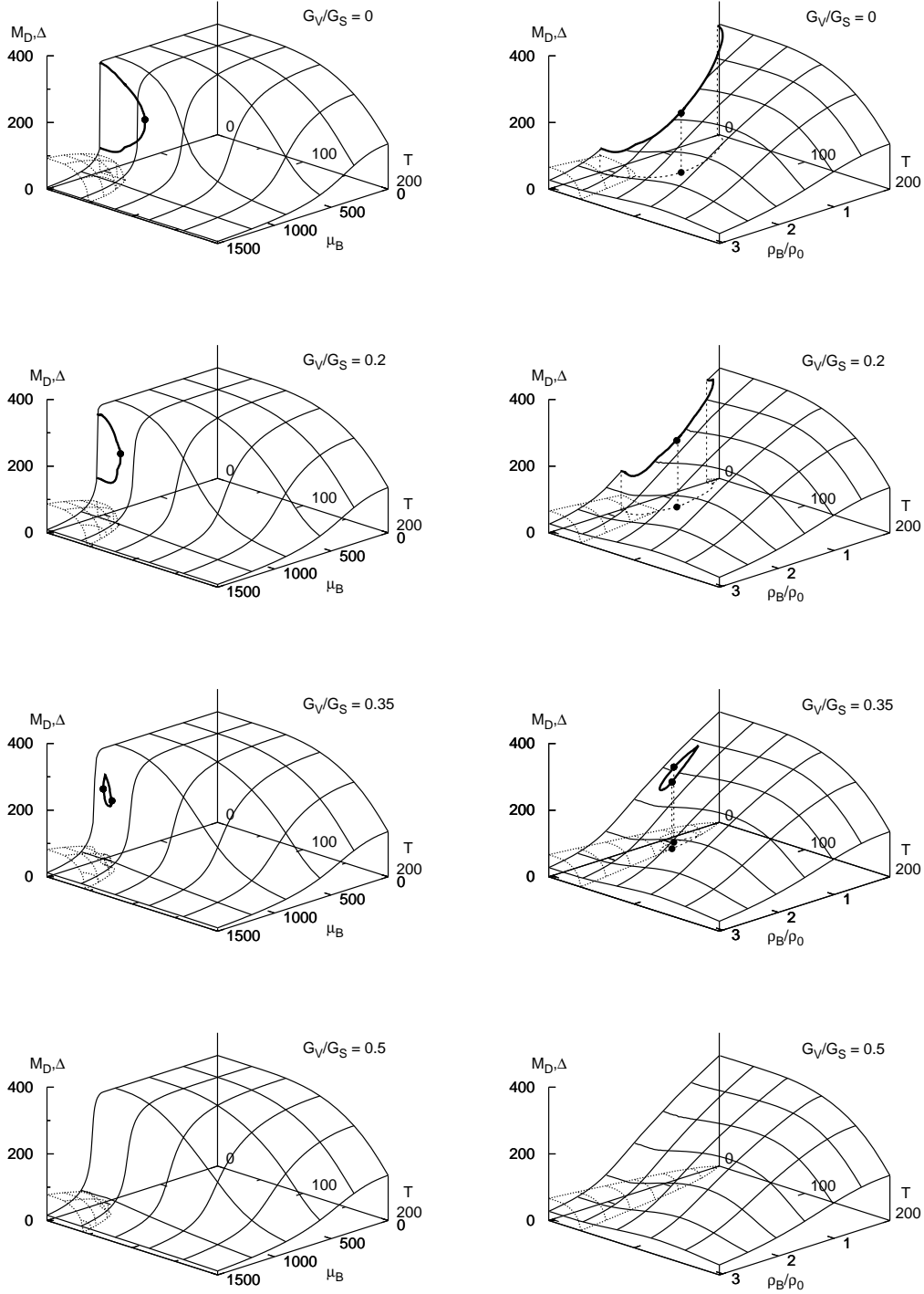


Fig. 12. The left panels show three-dimensional plots of the order parameters M_D (solid lines) and Δ (dashed lines) as functions of (T, μ_B) with various values of G_V/G_S , while the right panels show them as functions of (T, ρ_B) . The thick line corresponds to the first-order transition and the circles denote their endpoints. Notice that the behavior of the order parameters as functions of (T, ρ_B) does not depend on G_V , except in the region of the mixed phases, in accordance with the discussion given in §3.

(CSC) phases: The first-order transition between the χ SB and CSC phases becomes weaker as the vector coupling is increased, and there can exist two endpoints of the critical line of the first-order restoration in some range of parameters values; the two endpoints become tricritical points in the chiral limit. Our calculation has shown that the repulsive vector interaction enhances the competition between the χ SB and CS phases, leading to a degeneracy in the thermodynamic potential in the M_D - Δ plane. This implies that there exists gigantic fluctuations of the order parameters that appear in a correlated way near the critical region, and it suggests the necessity of a theoretical treatment incorporating the fluctuations. This is, however, beyond the scope of this work. We have found that the coexisting phase, in which the quarks with dynamically generated mass are color-superconducting, appears in a wide range of values of μ_B and T . Here it should be emphasized that it is not yet known whether the chiral and the confinement-deconfinement transitions occur simultaneously at finite density; hence there may exist quark matter with chiral symmetry breaking. We have emphasized that the appearance of such a coexistence phase becomes robust and hence universal through the inclusion of the vector interaction. We have also shown that the repulsive vector interaction causes the transition from the chirally broken phase to color superconducting phase to move toward larger μ_B .

Although our analysis is based on a simple model, our finding that the vector interaction enhances the competition between the χ SB and CSC phase transitions is universal and should be confirmed and further studied with more realistic models, including the random matrix model and on lattice QCD. In fact, phase structure similar to that found here has been obtained in two-color QCD on the lattice,^{7),8)} in which there appear two tricritical points related to the chiral and CSC transitions, and also the coexisting phase in a wide range of the temperature and chemical potential. It may be possible to intuitively understand these results in terms of the effective vector coupling, which can be extracted by calculating the baryon-number susceptibility. A random matrix study of the QCD phase diagram^{62),65)} incorporating the vector condensate (i.e., the density) explicitly should be carried out.

In this work, we have ignored color neutrality in the CSC phase.^{69)–72)} It is known, however, that color neutrality seems to have an only small effect on the onset of CS: When the superconducting gap is sufficiently smaller than the Fermi momentum, as is the case in a wide region of the T - μ plane in our calculation, the densities of the paired and unpaired quarks are close in magnitude. Therefore, the present results obtained for the effects of the vector coupling will only slightly change when the color neutrality is taken into account, although the two-end-point structure, which is realized through a delicate interplay between χ SB and CS through the vector coupling, might disappear or persist in the mean-field approximation we have employed.

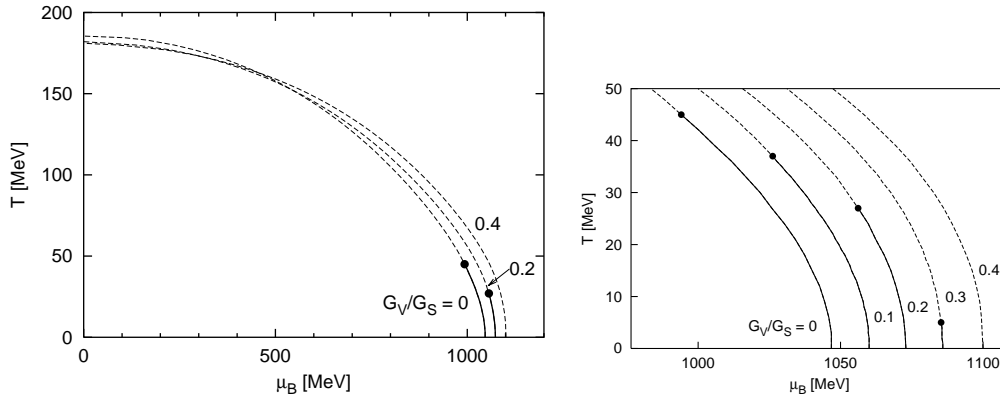


Fig. 13. The G_V dependence of the phase diagram for the chiral transition in the T - μ plane. The solid line represents the critical line of the first-order transition. The dash-dotted line denotes an artificial critical line of the crossover transition, which is determined with the same condition as that stated in the text.

In the two-flavor case which we have treated in this paper, the first two-color states which form the color Cooper pairs should have different dynamical mass from the remaining color state. Although incorporating such color-dependent dynamical masses^{(24),(29),(48)} is known to import only a tiny effect, it should be taken into account for a complete analysis of the effects of the vector coupling on the phase boundaries.

Furthermore, when applying the theory to neutron star phenomena, the charge neutrality and the beta equilibrium condition incorporating degenerate neutrinos^{(70),(71)} should also be taken into account. We have confined our investigation to the two-flavor case in this work. Needless to say, it would be very interesting to examine the effects of the vector interaction in the three-flavor case, and thereby on the color-flavor locked phase.^{(25)–(28)}

T.Kunihiro thanks David Blaschke for informing him of the work by Buballa et al.⁽⁴⁸⁾ and related papers after the completion of this work in May. We are grateful to Michael Buballa for pointing out us some misleading statements in the original manuscript with regard to Ref. 48) and subsequent discussions for elucidating the relation between the present work and Ref. 48). M. Kitazawa thanks H. Abuki for communications confirming the precise meaning of his master thesis.⁽⁶⁴⁾ This work is partially supported by Grants-in-Aid from the Japanese Ministry of Education, Science and Culture (No. 12640263 and 14540263).

Appendix A

— *Effects of the Vector Interaction on the Chiral Phase Transition* —

In this appendix, we summarize how the chiral transition is affected by the vector interaction in the case that the CS is not incorporated. Although this problem has been examined

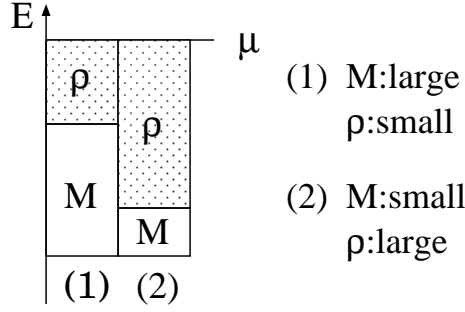


Fig. 14. A conceptual diagram accounting for the relation between the total quark mass $M = m + M_D$ and the density ρ_q at given μ_q . The quark density in the equilibrium state becomes small for larger M with μ_q fixed.

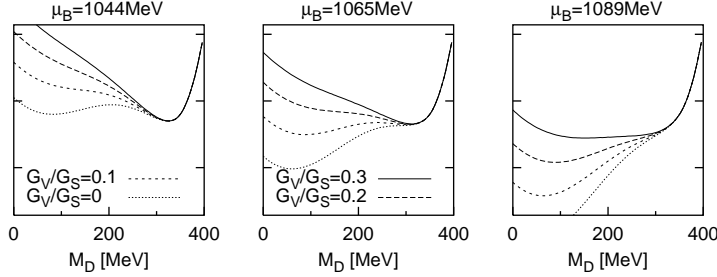


Fig. 15. The thermodynamic potential at $T = 0$ as a function of M_D for $G_V = 0, 0.1, 0.2, 0.3$. For smaller G_V , ω has two local minima, reflecting a first-order transition. As G_V is increased, ω_D at small M_D becomes large and the local minimum at smaller M_D disappears. In this way, the chiral transition becomes a crossover.

by some authors,^{23),46)} no coherent summary has been given in the literature.

The phase diagram of the chiral transition in the T - μ plane is shown in Fig. 13. Here we have used the same Lagrangian (2.3) as that used in the text, but with G_C switched off. One can see the following features from Fig. 13:

- (i) The chiral restoration is shifted toward larger μ as G_V is increased.
- (ii) G_V acts to moves the endpoint toward lower T and larger μ .
- (iii) The chiral restoration eventually turns into a crossover transition for large G_V .

The feature (i) can be understood as follows. The Fermi momentum $p_F = \sqrt{\mu^2 - M^2}$ becomes large (small) for small (large) M , where $M = m + M_D$ is a constituent (total) quark mass, and so does the density ρ at the fixed μ (see Fig. 14). Since the vector interaction gives rise to a repulsive energy proportional to the density squared, $G_V \rho_q^2$, a system with a smaller density is favored when G_V is present. Thus one can see when G_V is finite, the larger M is favored. We show the thermodynamic potential ω as a function of M_D with various G_V in Fig. 15. We see that the thermodynamic potential at small chiral condensate M_D

increases as G_V increases, owing to the repulsion of the vector interaction. Accordingly, the chiral restoration is shifted toward large μ as G_V is increased.

Figure 15 also shows that the first-order transition is weakened as G_V is increased: One sees from the far left panel that the thermodynamic potential with $G_V = 0$ has two local minima and there exists a bump between these minima. This two-local minima structure becomes less prominent and the local minima becomes closer as G_V is increased (see the $G_V/G_S = 0.2$ case (short-dashed line) in the middle panel). Such two-local minima structure disappears at $G_V = 0.3$ for all μ_B .

References

- 1) C. Detar, in Quark Gluon Plasma 2 ed. by R. C. Hwa(World Scientific 1995).
- 2) F. Karsch, Lect. Notes Phys. **583**, 209 (2002).
- 3) A. Nakamura, Phys. Lett. **B149**, 391 (1984).
- 4) S. Muroya, A. Nakamura and C. Nonaka, Nucl. Phys. Proc. Suppl. **94**, 469 (2001).
- 5) Z. Fodor and S. D. Katz, Phys. Lett. **B534**, 87 (2002) ;JHEP **0203**, 014 (2002).
- 6) S. Hands, J. B. Kogut, S. E. Morrison and D. K. Sinclair, Nucl. Phys. Proc. Suppl. **94** 457 (2001); J. B. Kogut, D. K. Sinclair, S. Hands and S. E. Morrison, Phys. Rev. **D64**, 094505 (2001).
- 7) J. B. Kogut, D. Toublan and D. K. Sinclair, Phys. Lett. **B514**, 77 (2001).
- 8) J. B. Kogut, D. Toublan and D. K. Sinclair, hep-lat/0205019, and the references cited therein.
- 9) R. Alosio, V. Azcoiti, G. Di Carlo, A. Galante and A. F. Grillo, Nucl Phys **B606**, 322 (2001).
- 10) S. P. Klevansky, Rev. Mod. Phys. **64**, 649 (1992).
- 11) T. Hatsuda and T. Kunihiro, Phys. Rep. **247**, 221 (1994).
- 12) T. Schäfer and E. Shuryak, Rev. Mod. Phys. **70**, 323 (1998).
- 13) J. I. M. Verbaarschot and T. Wettig, Ann. Rev. Nucl. Part. Sci. **50**, 343 (2000).
- 14) B. Barrois, Nucl. Phys. **B129**, 390 (1977).
- 15) D. Bailin and A. Love, Phys. Rep. **107**, 325 (1984).
- 16) M. Iwasaki and T. Iwado, Phys. Lett. **B350**, 163 (1995); Prog. Theor. Phys. **94**, 1073 (1995).
- 17) M. Alford, K. Rajagopal and F. Wilczek, Phys. Lett. **B422**, 247 (1998).
- 18) R. Rapp, T. Schäfer, E. V. Shuryak and M. Velkovsky, Phys. Rev. Lett. **81**, 53 (1999).
- 19) R. D. Pisarski and D. H. Rischke, Phys. Rev. Lett. **83**, 37 (1999).
- 20) D. T. Son, Phys. Rev. **D59**, 094019 (1999).

- 21) T. Schäfer and F. Wilczek, Phys. Rev. **D60**, 114033 (1999).
- 22) R. D. Pisarski and D. H. Rischke, Phys. Rev. **D61**, 051501 (2000).
- 23) J. Berges and K. Rajagopal, Nucl. Phys. **B538** 215 (1999).
- 24) R. Rapp, T. Schäfer, E. V. Shuryak and M. Velkovsky, Ann. Phys. **280**, 35 (2000).
- 25) M. Alford, K. Rajagopal and F. Wilczek, Nucl. Phys. **B537**, 443 (1999).
- 26) M. Alford, J. Berges and K. Rajagopal, Nucl. Phys. **B558**, 219 (1999).
- 27) M. Buballa and M. Oertel, Nucl. Phys. **A703**, 770 (2002).
- 28) F. Gastineau, R. Nebauer and J. Aichelin, Phys. Rev. **C65**, 045204 (2002).
- 29) M. Harada and S. Takagi, Prog. Theor. Phys. **107**, 561 (2002).
- 30) K. Rajagopal and F. Wilczek, Chapter 35 in the Festschrift in honor of B. L. Ioffe, "At the Frontier of Particle Physics / Handbook of QCD", M. Shifman, ed., (World Scientific).
- 31) M. Alford, Ann. Rev. Nucl. Part. Sci. **51**, 131 (2001).
- 32) M. Kitazawa, T. Koide, T. Kunihiro and Y. Nemoto, Phys. Rev. **D65**, 091504(R) (2002).
- 33) R. D. Pisarski and D. H. Rischke, Nucl. Phys. **A661**, 205 (1999).
- 34) Y. Nambu and G. Jona-Lasinio, Phys. Rev. **122**, 345 (1961); **124**, 246 (1961).
- 35) T. Kunihiro, Nucl. Phys. **B351**, 593 (1991).
- 36) M. Asakawa and K. Yazaki, Nucl. Phys. **A504**, 668 (1989).
- 37) T. Eguchi and H. Sugawara, Phys. Rev. **D10** (1974), 4257;
- 38) H. Kleinert, Phys. Lett. **B59** (1975), 163; *ibid.* **B62** (1976), 429;
- 39) D. Ebert and H. Reinhardt, Nucl. Phys. **B 271** (1986), 188;
- 40) M. K. Volkov, Part. and Nuclei, **24** (1993), 81.
- 41) V. Berbarud, U. -G. Meissner, and I. Zahed, Phys. Rev. **D36**, 819 (1987).
- 42) S. Klimt, M. Lutz and W. Weise, Phys. Lett. **B249**, 386 (1990).
- 43) M. Lutz, S. Klimt and W. Weise, Nucl. Phys. **A542**, 521 (1992).
- 44) T. Kunihiro, Phys. Lett. **B271**, 395 (1991).
- 45) D. Evert, Yu. L. Kalinovsky, L. Munchow and M. K. Volkov, Int. J. Mod. Phys. **A8**, 1295 (1993).
- 46) M. Buballa, Nucl. Phys. **A611**, 393 (1996).
- 47) K. Langfeld and M. Rho, Nucl. Phys. **A660**, 475 (1999).
- 48) M. Buballa, J. Hošek and M. Oertel, Phys. Rev. **D65**, 014018 (2001).
- 49) T. Kunihiro, in *CONFINEMENT 2000* ed. by H. Suganuma, M. Fukushima and H. Toki, (World Scientific, 2001), p. 287; hep-ph/0007173.
- 50) N. Evans, S. D. H. Hsu and M. Schwetz, Nucl. Phys. **B551**, 275 (1999).
- 51) T. Schäfer and F. Wilczek, Phys. Lett. **B450**, 325 (1999).

- 52) M. Kitazawa, T. Koide, T. Kunihiro and Y. Nemoto, an oral talk in JPS meeting at Ritsumeikan University, Kusatsu (April, 2002); see also M. Kitazawa, Master thesis submitted to Kyoto university, in Japanese, (February, 2002).
- 53) U. Vogl and W. Weise, Prog. Part. Nucl. Phys. **27**, 195 (1991).
- 54) D. Evert, H. Reinhardt and M. K. Volkov, Prog. Part. Nucl. Phys. **33**,1 (1994)
- 55) R. Alkofer and L. von Smekal, Phys. Rep. **353**, 281 (2001).
- 56) T. M. Schwarz, S. P. Klevansky and G. Papp, Phys. Rev. **C60**, 055205 (1999).
- 57) As a recent work, H. Mineo, W. Bentz, N. Ishii and K. Yazaki, Nucl. Phys. **A703**, 785 (2002).
- 58) See for example, J. D. Bjorken and S. D. Drell, *Relativistic Quantum Fields*, p.116 (McGraw-Hill, 1965).
- 59) B. D. Serot and J. D. Walecka, Advance in Nuclear Physics, Vol. 16, PLENUM PRESS NEWYORK-LONDON (1986).
- 60) C. W. Carter and D. Diakonov, Phys. Rev. **D 60**, 016004 (1999).
- 61) H. Mishra and J. C. Parikh, Nucl. Phys. **A679**, 597 (2001).
- 62) B.Vanderheyden and A.D.Jackson, Phys. Rev. **D62**, 094010(2000).
- 63) Mei Huang, Pengfei Zhaung, Weiqin Chao Phys.Rev. **D65**, 076012 (2002).
- 64) H. Abuki, Master thesis submitted to Kyoto university, in Japanese, (2000).
- 65) B.Vanderheyden and A.D.Jackson, Phys. Rev. **D64**, 074016 (2001).
- 66) G. E. Brown and M. Rho, Phys. Rep. **269**, 333 (1996).
- 67) M. Harada, Y. Kim, M. Rho and C. Sasaki, hep-ph/0207012.
- 68) G. Boyd, S. Gupta, F. Karsch and E. Laermann, Z. Phys. **C 64**, 331 (1994).
- 69) K. Iida and G. Baym, Phys. Rev. **D 63**, 074018 (2001).
- 70) M. Alford and K. Rajagopal, hep-ph/0204001.
- 71) A. W. Steiner, S. Reddy and M. Prakash, hep-ph/0205201.
- 72) M. Huang, P. Zhuang and W. Chao, hep-ph/0207008.